

# Interactive 3D Segmentation of Lymphatic Valves in Confocal Microscopic Images

Jonathan-Lee Jones, Xianghua Xie\*

Department of Computer Science, Swansea University, Singleton Park, Swansea, UK.

\*x.xie@swansea.ac.uk <http://cvision.swan.ac.uk>

**Abstract.** We present a novel method of segmentation of lymph valve leaflets from confocal microscopy studies. By using a user informed, layer based segmentation framework, we segment the outer boundary of the lymph valve in 3D from a series of confocal images. This boundary is then used to compute the surface structure of the vessel by providing a boundary constraint to a dual graph based on minimum surface segmentation. This segmentation creates a point cloud of voxels on the surface of the valve structure, we then apply an RBF interpolation to reconstruct it as a continuous surface.

## 1 Introduction

The lymphatic system is vital for maintaining healthy functionality in the body; fulfilling this task by the transport of fluids and immunological cells from and to the blood and interstitial spaces. The lymphatic system at its most basic is a system of pipes and valves to ensure unidirectional flow, but unlike the cardiovascular system it is not a pressurised closed system. Failure of the lymphatic system leading to lymphedema is a common complication in several disease states, and is a detrimental factor in recovery and improving quality of life in post operative patients. Texture analysis and deformable modelling, e.g. [12, 14, 13] may be applied to segment the vessel borders. The focus of this paper is to investigate the lymph valve structures, using computer imaging techniques to reconstruct the valve in 3D from *ex vivo* confocal microscopic image series. There has been little investigation of the lymphatic system in general, and even less on the valve structures. Segmenting the valves is a challenge, as they are small delicate structures and whereas finding the tip of the valve is relatively less ambiguous, the hinge region presents a significantly greater difficulty. Fig. 1 provides example slices.

There is a great deal of interest in methods to find a minimal surface in 3D, Appleton [1] suggested, for example, a method of solving a continuous max-flow algorithm, whereas other methods have been put forward using geometric constraints [8], regional properties [4], and shape priors [9] to give but a few examples. Unlike in 2D segmentation, minimal surfaces must always be closed, with boundary constraints applied. They can be thought of like blowing a soap bubble, with the ring used to blow the bubble as the boundary constraining it,

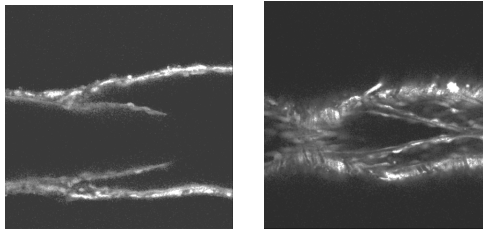


**Fig. 1.** Processed data showing the valve structure in a single data set. Notice how the shape and quality of the image changes from the slice on the periphery of the valve (right image) compared to a slice from the mid region (on the left).

and the bubble itself as the surface. By using an adaptation of our 2D method [6] into 3D, we can provide a boundary to meet the second constraint criteria required for minimal surface segmentation. This will be combined with the graph construction to provide segmentation of the surface as a whole. It is important when working in 3D to consider surfaces rather than direct shortest paths [2, 10, 11, 7] as it is a well known phenomenon that the shortest path between two points, does not necessarily correspond to a path on the minimal surface between two closed shapes. We will apply interactive methods to allow expert knowledge to guide the difficult segmentation of the valve, and then use this user guided boundary to automatically segment the surface of the valve.

## 2 Proposed Method

Briefly, the proposed method first localise the outer boundaries of the lymph leaflets in 3D using an interactive segmentation method and then computes a complete 3D surface using a minimal surface algorithm. The user input is simplistic interaction by clicking a few points indicating a small number of points along the border. This interactive segmentation in 3D is an extension of our previous 2D method [6]. The user input is treated as a soft constraint, rather than a hard constraint, i.e. the segmentation does not necessarily pass the user points. This is achieved by finding a shortest path in a layered 3D graphs. The localised borders of the lymph leaflets are then used as boundary constraints for computing a minimal surface using a primal dual algorithm in discrete optimisation.

### 2.1 User input

The user input is used to assist in labelling the root and tip of the valve. This is done using an adaptation of the imprecise user input which we have used previously in our 2D segmentation method [6]. User points are placed corresponding to the tip and the hinge points on the valve itself. These user points are used to find the valve boundary, which will be used to find the surface of the valve. The

segmentation forms a closed curve starting and finishing in the same point, circumscribing the boundary of the valve. This user input is effective but minimal and allows imprecision in user point placement which is desirable in 3D.

## 2.2 Graph construction

In this graph, the 3D structure  $\mathcal{I}$  is a representation made up from multiple layers  $\mathcal{L}$  constructed from the sequential slices of the confocal series. The number of layers used is  $2h$  where  $h$  is the number of slices in the confocal image series. The graph structure is made up of the slices  $s$  from  $s_1$  to  $s_n$ , then the layers are replicated in reverse order (adding slices  $s_n$  to  $s_1$ ), to construct a cube of twice the height of the original image stack. We construct a graph  $G = (V, E)$ , where  $V$  is the set of vertices, and  $E$  the set of weighted edges. For each voxel  $v$ , there exists an edge  $e$  to each of its neighbouring pixels on the same layer and to its neighbour in the subsequent layer. Therefore, a pair of neighbouring voxels  $(p, q) \in V$  with a corresponding edge  $e = (v_p, v_q)$  also have an edge to the corresponding point on the superseding layer  $e = (v_{p_l}, v_{q_{l+1}})$ , where  $l$  represents the current layer of the image. For each edge, we assign a weight  $w$  to build a weighted graph  $(V, E)$ . These weights are calculated based on whether the edge is internal to a layer ( $w_i$ ) or trans-layer ( $w_x$ ). In order to be able to solve this problem in polynomial time, we enforce an order (as previously for the 2D method) moving through the image from  $l_1$  to  $l_{2n}$  where  $n$  is the depth of the image cube, and layers  $l_1$  to  $l_n$  represent moving through the images using the tip terminal point as a guide, then layers  $l_{n+1}$  to  $l_{2n}$  are returning using the hinge terminal point. This is done by ensuring that the inter-layer arcs are unidirectional. We use the user points as elastic soft constraints to help guide the segmentation.

User points are placed for both the ends of the valve (the tip and the hinge), and the source  $s$  is the tip point on layer 1 and sink  $t$  is set to the same point (as we need to create the full closed outline of the valve) but on layer  $l_{2n}$ , we also place user points on the ends of the valve for each layer to act as guide in the segmentation.

Edges of zero weight are not added from the start node  $s$  to each pixel in the first layer, and from the last layer  $2n + 1$  to the terminal node  $t$ , making sure the first and the last user points elastic and not hard constraints, and all user points are treated equally.

If  $P$  is the set of pixels in the image,  $P_s$  is therefore the subset of pixels that also fall on the boundaries of our super pixels, and  $p_i$  and  $q_i$  are pixels in layer  $i$  giving  $v_{p_i}$  as the vertex  $p$  in layer  $i$ , we can define the set of nodes  $V$  as  $V = \{s, t\} \cup \{p_i \in P_s \wedge 1 \leq i \leq k + 1\}$  and thusly the set of edges as,

$$E = \begin{cases} (s, v_{p_1}) | p \in P_s & \cup \\ (v_{p_{k+1}}, t) | p \in P_s & \cup \\ (v_{p_i}, v_{q_i}) | (p, q) \in N \wedge 1 \leq i \leq k + 1 & \cup \\ (v_{p_i}, v_{p_{i+1}}) | p \in P_s \wedge 1 \leq i \leq k + 1. & \end{cases} \quad (1)$$

### 2.3 Valve Boundary Detection

The first stage of our valve leaflet segmentation is to segment the boundary. Using the constructed graph  $G$  and manually labelled points for the apex and root of the valve, we assign weights to the edges in a similar manner as before. The edges on the directed layered graph are categorised as internal edges  $w_i$  within individual layers and inter-layer edges  $w_x$ . The weighting for these two types of edges is assigned differently. The internal edges are assigned weights based on edge features, i.e. boundary based edge weights similar to the 2D method are used, but not region based edge weights. The boundary based edge weights are calculated based on the magnitude of image gradients, i.e. using an edge detection function  $g_e = 1/(1 + \nabla I)$  where  $I$  denotes the pre-processed image. Hence, for any given edge between neighbouring pixels  $(v_p, v_q)$ , we assign a weight ( $w_e$ ) according to

$$w_i((v_p, v_q)) := \frac{1}{2} \|p - q\| (g_e(p) + g_e(q)). \quad (2)$$

The attraction force imposed by user points is materialised through the inter-layer edge weights  $w_x$ . We apply distance transform to the user points in each layer of the graph, and the inter-layer edge weight is assigned as  $w_x = d(v_{p_i}, v_{p_j})$  where  $d$  denotes the distance transform function. For layers  $l_1$  to  $l_n$  we use the user points corresponding to the tip, and layers  $l_{n+1}$  to  $l_{2n}$  use the user points derived from the hinges. In this way, distance weighting produces iso-linear bands of weight around each user point, with increasing weight to go through to the next layer as the distance from the user point increases, favouring transition between layers as close as possible to the user point without straying too far from hard edges. In this way, finding the boundary of the valve becomes an energy minimisation problem similar to our previous 2D work [6].

The energy function for any curve  $C$  in our method is a combination of two terms, i.e. for any arc  $C$  between two points  $p_i$  and  $p_j$ ,  $C(p, q) = w_x + w_i$ , where  $w_x$  can be written as  $\alpha \sum_{i=1}^k \|C(s_i) - X_i\|$ , and  $w_i$  can be formulated as:  $\beta \int_0^{L(C)} g(C(s)) ds$ . This is all providing that the points are treated as being in a sequential order, and that the interconnections between layers are uni-directional. The overall energy function can then be expressed as:

$$\begin{aligned} \mathcal{E}(C, s_1, \dots, s_k) = & \alpha \sum_{i=1}^k \|C(s_i) - X_i\| \\ & + \beta \int_0^{L(C)} g(C(s)) ds \quad s.t. s_i < s_j, \forall i < j. \end{aligned} \quad (3)$$

where  $\alpha$  and  $\beta$  are real constants used to weigh the effects of the edge based and distance based terms.

The first term in our cost equation is used to enforce the soft constraints placed by the user as a guideline to the terminal ends of the valve, and it penalises

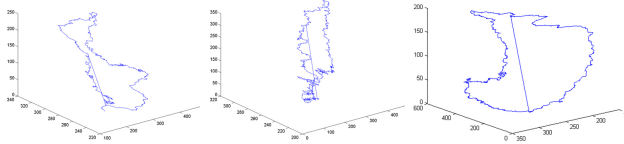


**Fig. 2.** 3D Segmentation of the boundary of the valve leaflets.

the paths further away from these user points, helping the user control the segmentation. The second term is the boundary based data term that prefers the path passing through strong edges, the images are preprocessed to improve these images as described above. By using the layered graph construction, the minimisation of the energy function is achieved by finding the shortest path from the start point  $s$  to the end point  $t$  through the 3D graph.

As the graph will be very large, and therefore computationally expensive, the graph was constructed in segments. By using Dijkstra’s algorithm, this allowed the points on the graph to be loaded in as needed, we operated on 10 layers at a time, as this provided a sufficient reduction in the size of graph. To further reduce the computational overheads, the image was automatically cropped to a tight box around the region of the valve, by using the manually input points to give a rough boundary, which was expanded in each direction to ensure the valve fitted within these confines in its entirety. Note, the inter-layer edges are unidirectional so that the path can not travel back to previously visited layers, to avoid making the segmentation problem NP hard. The results of this 3D segmentation, gave the boundary outline for the valve leaflet (see Fig. 2).

## 2.4 Valve Surface Segmentation

Once we obtain the boundary, the next stage is to calculate the point cloud for points on the surface of the valve. For this, the image stack was comprised of layers  $l_1$  to  $l_n$ , where  $n$  is the number of slices in the series. Note this is a smaller graph than that is used for the border, as there is no need to have the  $2n$  layers to ensure order in the user points. This is done using the voxel edge derived intensities for any given voxel  $v$  in the image stack, that are based on the edge map. A minimal surface segmentation performed using these weights, based on the method demonstrated in [5], with adapted cost functions.

The first stage is to construct a lattice framework to represent the 3D image. We first expand our original graph construction into a dual graph. From our planar primal graph, we define a dual graph by replacing each node with a facet, can connecting two nodes if their respective facets share an edge.

We can therefore define our lattice using the same connectivity used to construct the graph for boundary segmentation, namely with nodes being connected to their 8 neighbours on their layer, and immediate neighbour nodes on the layer above and below themselves. The lattice can be represented by

set  $P = (V, E, F, C)$  where the vertices  $v \in V$ , edges  $e \in E \subseteq V \times V$ , facets  $f \in F \subseteq E \times E \times E \times E$  and cubes  $c \in C \subseteq F \times F \times F \times F \times F \times F$ , if we work with a 6 connected neighbourhood. For any given edge  $e_i$  we assign a weight  $w_i$ , with all weights being positive.

The minimum surface weight problem can therefore be defined as:  $\min_z Q(z) = \sum_i w_i z_i$ , subject to  $Bz = r$ , where  $z$  is a positive vector indicating whether the facet is present in the minimal-weight surface.  $w_i$  is the weight of the facet, which corresponds to the weight of the edge in the 2D graph, and is defined as:

$$w_i = \alpha \sum_{i=1}^k \|C(s_i) - X_i\| + \beta \int_0^{L(C)} g(C(s)) ds \quad (4)$$

and  $B$  is the incidence matrix boundary operator and  $r$  is a signed vector indicative of a closed contour. Once the problem is formulated, it can be resolved by using a Minimum-cost Circulation Flow Network (MCFN) based on work by Bitter *et al* [3]. This can be formed in terms of the variable  $f$ :

$$\max_{f'} z_0^T f', \text{ s.t. } C^T f' = 0, f' \leq \tilde{f} = w. \quad (5)$$

which requires the finding of the maximum divergence-free flow, passing through an initial surface  $z_0$ , which has the capacities given by the weights in the graph.

Once the MCFN has been solved, the results show facets that are to be included in the final solution. It is then a trivial task to deconstruct the dual lattice back to its primal roots and generate a node representing the centre of the volume indicated by the facet. These nodes will then be used to generate the final result by having a 3D RBF interpolation applied to them, to smooth outliers and provide a smooth surface which represents the valve itself.

### 3 Results

Our results were obtained from a data-set of five confocal series, from different lymph valves. These individual datasets each comprised of around 400 consecutive images of the lymph valve. These were used to construct the point cloud and surfaces. The point clouds represent voxels on the surface of the valve. Finding the surface for the valve is challenging, as the leaflets are very faint, and often merge into the wall, or exit the side of the frame. Some of the effects can be seen in the alternate views shown in Fig. 1. Furthermore, in order to obtain a coherent surface over these point clouds it is necessary to perform smoothing and RBF interpolation on the clouds. The results from the minimal surface segmentation are shown in Fig. 3, with a colour map applied to show the bands obtained from the RBF centres. The RBF centres for interpolation were taken at regular intervals (10 slices) through the image, as this provided an adequate smoothing to produce a surface, whilst keeping the computational overheads small so the operation is fast, and the resultant image manageable.

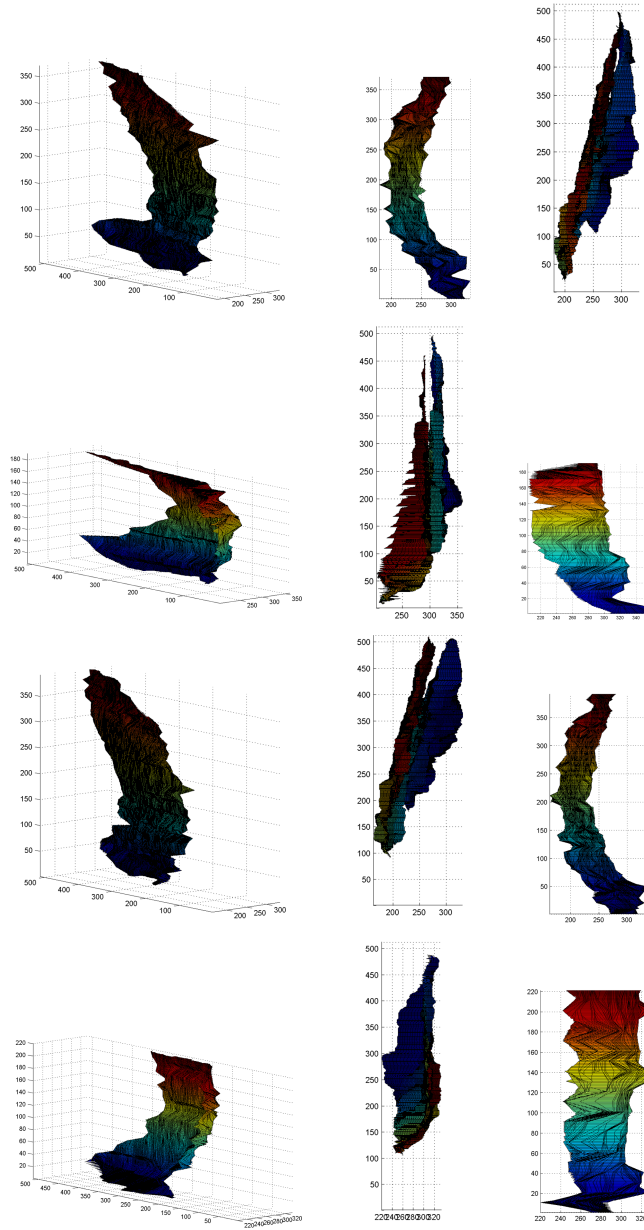


**Fig. 3.** 3D Segmentation results, showing the surface mapped over the point clouds. Coloured bands represent the regions used for the RBF interpolation. From left to right they are: an off centre view displaying the valve structure, X-Y, and X-Z planes, for each data-set.

The proposed method achieved good segmentation of the lymph valves. By using user input to inform the boundary segmentation, we avoid the imaging problems inherent in the data of this type. Namely the nature of the images make identification of terminal regions of the valve exceedingly difficult, especially in the early and late stages. As can be seen in the second image in Fig. 1, it is almost impossible to discern where the valve starts and finishes in these regions, and even in the selected regions, where the valve can be seen, it differs greatly in shape as you move through the slices. The proposed method for boundary segmentation shows the versatility to allow the user to place guide points without the necessity for extreme precision, allowing for user input even in regions where this is difficult. The proposed method builds on our previous 2D work in [6] through the modification of the graph construction to allow for 3D segmentation. The poor quality of the images, coupled with the changing shape and irregularity of the valve made segmentation difficult, but the proposed method manages to overcome these and provides a promising results.

## References

1. Appleton, B., Talbot, H.: Globally minimal surfaces by continuous maximal flows. *IEEE T-PAMI* 28(1), 106–118 (2006)
2. Armstrong, C.J., Barrett, W.A., Price, B.: Live Surface. In: *Volume Graphics* (2006)
3. Bitter, I., Kaufman, A., Sato, M.: Penalized-distance volumetric skeleton algorithm. *IEEE T-VCG* 7(3), 195–206 (2001)
4. Dou, X., Wu, X., Wahle, A., Sonka, M.: Globally optimal surface segmentation using regional properties of segmented objects. In: *IEEE CVPR* (2008)
5. Grady, L.: Minimal surfaces extend shortest path segmentation methods to 3d. *IEEE T-PAMI* 32(2), 321–334 (2010)
6. Jones, J., Xie, X., Essa, E.: Combining region-based and imprecise boundary-based cues for interactive medical image segmentation. *International Journal for Numerical Methods in Biomedical Engineering* 30, 1649–1666 (2014)
7. Krueger, M., Delmas, P., Gimel'farb, G.: On 3d face feature segmentation using implicit surface active contours. In: *International Conference on Image and Vision Computing*. pp. 1–6 (2008)
8. Li, K., Wu, X., Chen, D., Sonka, M.: Globally optimal segmentation of interacting surfaces with geometric constraints. In: *IEEE CVPR*. vol. 1, pp. 394–399 (2004)
9. Song, Q., Wu, X., Liu, Y., Sonka, M., Garvin, M.: Simultaneous searching of globally optimal interacting surfaces with shape priors. In: *IEEE CVPR* (2010)
10. Wagenknecht, G., Poll, A., Losacker, M., Blockx, I., Van der Linden, A.: A new combined live wire and active surface approach for volume-of-interest segmentation. In: *IEEE Nuclear Science Symposium*. pp. 3688–3692 (2009)
11. Wieclawek, W., Pietka, E.: Live-wire-based 3d segmentation method. In: *IEEE EMBC*. pp. 5645–5648 (2007)
12. Xie, X., Mirmehdi, M.: Texture exemplars for defect detection on random textures. In: *Pattern Recognition and Image Analysis*. pp. 404–413 (2005)
13. Xie, X., Mirmehdi, M.: Magnetostatic field for the active contour model: A study in convergence. In: *BMVC*. pp. 127–136 (2006)
14. Xie, X., Mirmehdi, M.: Texems: random texture representation and analysis. In: *Handbook of Texture Analysis*, chap. 4 (2008)